Steel and Composite Structures, *Vol. 28, No. 2 (2018) 251-266*
DOI: https://doi.org/10.12989/scs.2018.28.2.251

Experimental and analytical study on the shear strength of corrugated web steel beams

Samer Barakat * and Moussa Leblouba [a]

Department of Civil and Environmental Engineering, College of Engineering, University of Sharjah, Sharjah, United Arab Emirates

(*Received February 4, 2018, Revised April 26, 2018, Accepted May 14, 2018*)

Abstract. Compared to conventional flat web I-beams, the prediction of shear buckling stress of corrugated web steel beams (CWSBs) is not straightforward. But the CWSBs combined advantages of lightweight large spans with low-depth high load-bearing capacities justify dealing with such difficulties. This work investigates experimentally and analytically the shear strength of trapezoidal CWSBs. A set of large scale CWSBs are manufactured and tested to failure in shear. The results are compared with widely accepted CWSBs shear strength prediction models. Confirmed by the experimental results, the linear buckling analyses of trapezoidal corrugated webs demonstrated that the local shear buckling occurs only in the flat plane folds of the web, while the global shear buckling occurs over multiple folds of the web. New analytical prediction model accounting for the interaction between the local and global shear buckling of CWSBs is proposed. Experimental results from the current work and previous studies are compared with the proposed analytical prediction model. The predictions of the proposed model are significantly better than all other studied models. In light of the dispersion of test data, accuracy, consistency, and economical aspects of the prediction models, the authors recommend their proposed model for the design of CWSBs over the rest of the models.

Keywords: corrugated web; shear buckling; experimental results; analytical model

1. Introduction

Corrugated web steel beams (CWSBs) are composed of corrugated webs that are welded to a pair of plane flanges. The corrugation prevents the buckling failure of the web and increases its buckling capacity to a level comparable with a 12 mm thick plane one (Dubina *et al*. 2015). Because of the corrugations, the web has no ability to sustain longitudinal stresses (BS EN 1993-1-5:2006). The conventional assumption is to ignore the web's contribution to resist bending moment. Therefore, the corrugated web is assumed to carry shear forces only. (CWSBs) have combined advantages of lightweight and large spans with relatively low-depth and high load-bearing capacities. Due to the use of thin corrugated webs (1.5 to 3 mm), beams and girders with corrugated webs have significantly less weight compared to hot rolled profiles or welded I-sections.

The use of thinner webs in CWSBs resulted in an estimated cost savings of 10-30% in comparison with conventional fabricated sections and more than 30% compared with standard hot-rolled beams (Dubina *et al*. 2015). However, one important parameter that should be carefully considered when using corrugated web is the thermal residual stresses resulting from the welding process of the different parts. The presence of such residual stresses might reduce the flexural and shear capacities of the design.

The improvements of the fully automated fabrication process in the CWSBs industry made it possible to use a variety of web thicknesses (1.5-6 mm), beam heights (300-1500 mm), flange thicknesses (6-30 mm) and flange widths (120-450 mm), and beam lengths up to 16 m (Pasternak and Kubieniec 2010). These improvements had considerably extended the field of application of CWSBs to cover even short span bridges, tapered beams with machine-made web openings, and mobile-modular home construction (Driver *et al*. 2006, Hassanein and Kharoob 2013, Hassanein and Kharoob 2014, Kharoob and Hassanein 2015, Dubina *et al*. 2015). In addition to that, new automated solutions use galvanized cold-formed steel elements for the webs as well as the flanges, thus, providing high protection against corrosion, which is a considered one of the major issues in steel constructions.

The effect of web corrugation on the shear strength of CWSBs was the subject of many experimental and theoretical studies (Elgaaly *et al*. 1996, Driver *et al*. 2006, Yi *et al*. 2008, Sause and Braxtan 2011, Guo and Sause 2014, Hassanein and Kharoob 2014, Moon *et al*. 2009, Niea *et al*. 2013, Barakat *et al*. 2015, Leblouba *et al*. 2017a, b, Lu and Ji 2018). Elgaaly *et al*. (1996) carried out experimental and theoretical studies on several trapezoidal corrugated beams and concluded that the shear buckling of the web was the primary reason for the failure of beams. In addition, it was observed that the local shear buckling occurs in the presence of coarse corrugated webs while global buckling happens to the beams with densely corrugated webs.

*Corresponding author, Professor,
E-mail: sbarakat@sharjah.ac.ae
[a] Ph.D., E-mail: mleblouba@sharjah.ac.ae

ISSN: 1229-9367 (Print), 1598-6233 (Online)

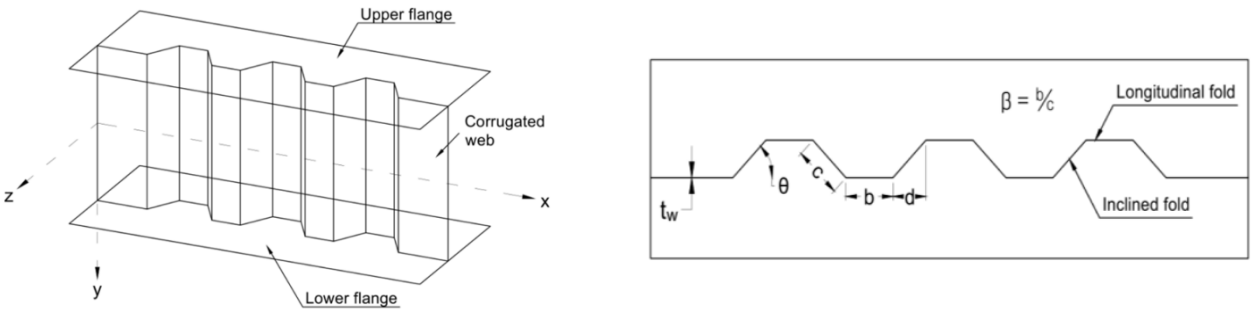

(a) (b)

Fig. 1 A CWSB and its geometric notations

Previous studies (Huang *et al*. 2004, Yi *et al*. 2008, Barakat and Leblouba 2018) demonstrated that the required shear strength is provided by the corrugated web, while the flanges provide the flexural strength to counter the accordion effect. However, the contribution of the corrugated web in resisting bending moments is almost negligible. As a result, no interaction is seen between shear and flexural behaviors (Ahmed 2005). Basinski (2018) reported the results of an experimental work on plate girders with sine-wave web corrugations. The aim was to investigate the effect of flexural stiffness of end stiffeners on the design of buckling resisting of the girders. The experimental work was strengthened with nonlinear finite element analysis. Basinksi concluded that rigid end stiffeners increase the shear buckling resisting of the girder by up to 11%, while failure of the web is related primarily due to the occurrence of tension line along the yield stress zones. As a result of this investigation, Basinski proposed a new method for the design of sine-wave corrugated web girders that take into account the rigidity of end stiffeners. Aggarwal *et al*. (2018) carried out a series of finite element analysis to investigate the local shear buckling of corrugated web beams. Finite element models of cantilever beams with different web geometries were analyzed using the commercial software ABAQUS. As a result of this investigation the authors developed a new equation was proposed and recommended to determine the local shear buckling coefficient, which should be used in the design of trapezoidal corrugated web beams.

This study aims at quantifying the effect of web corrugation on the increase in shear strength of the section in terms of the geometry of the corrugations and the properties of CWSBs. To that end, a set of shear-critical trapezoidal CWSBs are fabricated and tested to failure. The experimental results are added to the existing test database, which contains around 130 tests. New analytical prediction model accounting for the interaction between the local and global shear buckling of CWSBs is proposed in this work. The proposed model is tested against five previously published models using the test data collected by Sause and Braxtan (2011) and the experimental results of this study. The proposed model predicting accurately, yet conservatively, the critical shear buckling strength of CWSBs.

2. Shear buckling of corrugated webs

The corrugations in a CWSB may take many shapes: rectangular, triangular, semi-circular, sinusoidal, and trapezoidal. Fig. 1 illustrates a beam with trapezoidal corrugated web along with its geometric properties: the length of the horizontal corrugation (b), the length of the horizontal projection of the diagonal corrugation (d), the length of the diagonal corrugation (c), the corrugation angle (θ), and the thickness of the web (t_w).

Depending on the geometric properties, three shear buckling failure modes may take place in the corrugated webs: local, global, and interactive (or zonal as defined by Luo and Edlund 1996).

Shear buckling mode of failure occurs in thin corrugated webs when the shear forces carried by the web have not reached the full material's load carrying capacity (i.e., material strength). In other words, the shear stresses developed over the web plane, at the point of buckling

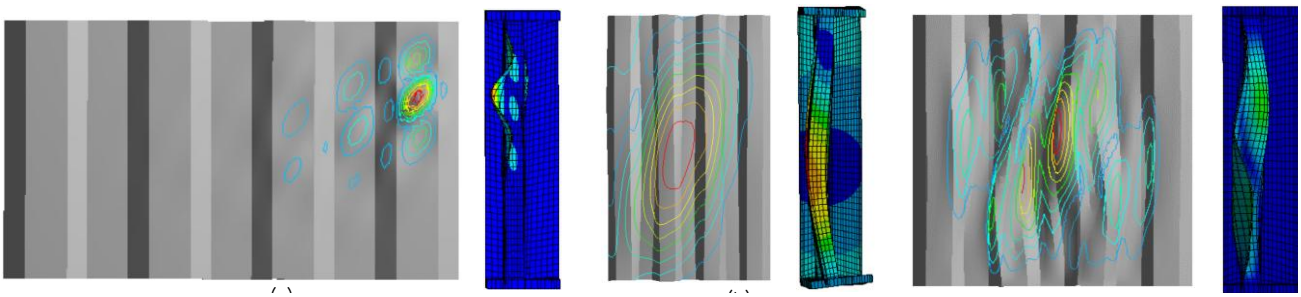

(a) (b) (c)

Fig. 2 Modes of shear buckling: (a) local; (b) global; (c) interactive

(bifurcation point), are less than the material ultimate shear stress. Buckling is associated with the loss of stability and depends mainly on the geometric properties of the thin web. Modeling of this phenomenon is usually done using linear buckling analysis (LBA), which involves the solution of the finite element Eigen-problem, where the elastic and geometric stiffnesses of the web component are the only required inputs. LBA can be used to predict the critical buckling load, defined by the load at which the web loses its stability under compressive stresses. The critical buckling load is obtained by multiplying the smallest eigenvalue, obtained using LBA, by the applied load.

To investigate the shear buckling of corrugated webs, three finite element models were prepared and analyzed using LBA. The geometric properties of the three specimens were selected carefully to observe the three modes of failure. Fig. 2 shows the results of the analyses. The local shear buckling mode (Fig. 2(a)) is shown to occur only in the flat plane folds of the web, while the global shear buckling (Fig. 2(b)) occurs over multiple folds of the web. Interactive shear buckling (Fig. 2(c)), on the other hand, defines a state of shear failure that is neither pure local, nor pure global buckling. Interactive shear buckling also involves several folds, but as shown in Fig. 2(c), it is localized only in a part of the web. Local buckling is considered to be controlled by the slenderness of the individual folds of the webs, whereas global buckling is considered to be controlled by the slenderness of the entire web (Moon *et al*. 2009, Sause and Braxtan 2011). However, if the local buckling extends from one fold to another, interactive buckling may take place, covering a larger number of corrugations, before global failure occurs due to the formation of a diagonal band under high tensile stresses.

In the subsequent sections different analytical models of the shear buckling stresses are presented. These models are categorized depending on the shear buckling mode.

2.1 Formulation for local shear buckling

Currently, the local shear buckling stress of a corrugated web is predictable using the plate buckling theory (Timoshenko and Gere 1961). According to this theory, the local elastic shear buckling stress τ_L is expressed as follows

$$\tau_L = k_L \frac{\pi^2 E}{12(1-\nu^2)(w/t_w)^2} \tag{1}$$

where k_L is defined as the local shear buckling coefficient and it depends on the aspect ratio of the folds and the boundary conditions of the beam, E is Young's modulus of the steel, ν is Poisson's ratio, w is the corrugation width, which changes from fold to fold. For longitudinal folds, $w = b$ (Fig. 1(b)), and for inclined folds, $w = c$. The larger of b and c is considered in calculating the τ_L. k_L, is the smallest when the ratio of w/h_w is small, where h_w is the height of the web. When the beam is simply supported, $k_L = 5.34$ and when clamped, $k_L = 8.98$ (Elgaaly *et al*. 1996).

2.2 Formulation for global shear buckling

Based on the orthotropic plate theory, Easley (1975) developed an analytical solution to the global shear buckling stress τ_G

$$\tau_G = k_G \frac{\left(D_y\right)^{1/4} \cdot (D_x)^{3/4}}{t_w \cdot h_w^2} \tag{2}$$

In Eq. (2), k_G is defined as the global shear buckling coefficient, which depends on the boundary conditions of the web. Elgaaly *et al*. (1996) recommended taking k_G as 31.6, assuming the flanges simply support the web, or 59, assuming the web is clamped to the flanges. D_x and D_y are the longitudinal and transverse bending stiffnesses calculated per unit length of the web, respectively, and they are defined for a trapezoidal corrugated web as follows (Sause and Braxtan 2011)

$$D_y = \frac{b+d}{b+d\cdot\sec(\theta)} \cdot \frac{E \cdot t_w^3}{12} \tag{3}$$

$$D_x = \frac{E}{b+d}\left(\frac{b \cdot t_w \cdot (d\cdot\tan(\theta))^2}{4} + \frac{t_w \cdot (d\cdot\tan(\theta))^3}{12\sin(\theta)}\right) \tag{4}$$

Elgaaly *et al*. (1996) have demonstrated that the formulas based on the plate buckling theory can predict, with reasonable accuracy, the shear strength of corrugated webs. However, Luo and Edlund (1996) compared the results obtained using nonlinear finite element analysis and found that the above formulations agreed well in only four out of fifteen analyzed beams. Of the four beams, two had dense corrugations and two had large overall dimensions.

In his Ph.D. dissertation, Abbas (2003) combined the three previous formulas to express the global shear buckling stress directly in terms of the geometric parameters shown in Fig. 1

$$\tau_{G,el} = k_G F(\theta,\beta)\frac{E t_w^{1/2} b^{3/2}}{12h_w^2} = C_G \frac{E t_w^{1/2} b^{3/2}}{12h_w^2} \tag{5}$$

where $F(\theta,\beta)$ is a coefficient determined based on the dimensions of the corrugations of the web

$$F(\theta,\beta) = \sqrt{\frac{1+\beta\sin^3\theta}{\beta+\cos\theta}} \cdot \left\{\frac{3\beta+1}{\beta^2(\beta+1)}\right\}^{3/4} \tag{6}$$

where $\beta = b/c$ and takes values between 1 and 2 (Sause and Braxtan 2011). Lower β corresponds to very deep corrugations that require more material, hence, uneconomical. Higher β corresponds to shallow corrugations that contribute very little to the overall shear buckling resistance of the beam. In addition, the corrugation angle, θ, is generally in the range of 30° to 45°, any smaller value would result in a situation where the web folds are no longer capable of supporting one another (Lindner and Huang 1995).

2.3 Formulation for interactive shear buckling

2.3.1 Previously published models

Most of the analytical models (Bergfelt and Leiva 1984, Linder and Aschinger 1988, El Metwally 1998, Shiratani *et al*. 2003, Ahmed 2005) developed to predict the interactive shear buckling stress, τ_I, have the following basic expression

$$\left(\frac{1}{\tau_I}\right)^n = \left(\frac{1}{\tau_L}\right)^n + \left(\frac{1}{\tau_G}\right)^n + \left(\frac{u}{\tau_y}\right)^n \quad (7)$$

where τ_y is the shear yield stress according to the Von Mises yield criterion, defined as

$$\tau_y = \frac{F_y}{\sqrt{3}} \quad (8)$$

in which F_y is the uniaxial yield stress of the web. The parameter u in Eq. (7) is set to zero when considering the interaction to be between local and global shear buckling only. In case of involvement of the shear yield stress, u takes non-zero values.

Several studies dealt with the interactive shear buckling considering that a possible interaction between the shear yield stress and shear buckling (i.e., $u \neq 0$). Among those is El-Metwally (1998) who assumed $n = 2$ and $u = 1$ in Eq. (7), Ahmed (2005) who assumed $n = 3$ and $u = 1$, and Sause and Braxtan (2011) who assumed $n = 3$ and $u = 2$.

Sause and Braxtan (2011) compared their own analytical model and other models with results collected from eight different studies. Altogether, these studies provided 102 different test data points. However, they had to omit all but 22 of these data points in their study because their respective test conditions were not compatible with the theories on which their model was based. More specifically, they omitted all data points that did not fall within the following parameter limits: (1) $a/h_w > 1$; (2) $\alpha \geq 22°$; and (3) $0.87 \leq \beta \leq 1.13$. Therefore, the model developed by Sause and Braxtan (2011) is applicable only to a limited category of CWSBs. In the range of applicability of their model, Sause and Braxton (2011) demonstrated that their model is more accurate than those proposed by El-Metwally (1998) and Yi *et al*. (2008).

In addition, many researchers accounted only for the elastic interactive shear buckling, hence the interaction would take place only between the local and global shear buckling ($u = 0$). Among those are Bergfelt (Bergfelt and Leiva 1984), Yi *et al*. (2008), and Barakat *et al*. (2015) who assumed $n = 1$, Abbas (2003) assumed $n = 2$, and Shiratani *et al*. (2003) assumed $n = 4$, in Eq. (7).

2.3.2 Proposed model

Based on 93 data points of the 102 test results collected by Sause and Braxtan (2011), Barakat *et al*. (2015) developed a new model to estimate the normalized interactive shear buckling strength. The model was established based on multiple regression analysis and had passed successfully both the *F*- and *t*-tests. The original version of the model gives the normalized shear buckling strength as a function of the interactive slenderness ratio, $\lambda_{I,1}$

$$\rho_{S1} = \frac{\tau}{\tau_y} = \frac{0.747}{\lambda_{I,1}} \quad (9)$$

Rearranging the terms in Eq. (7) to reach the interactive slenderness ratio $\lambda_{I,n}$

$$\lambda_{I,n} = \sqrt{\frac{\tau_y}{\tau_{I,n,el}}} = \lambda_L \lambda_G ((1/\lambda_L)^{2n} + (1/\lambda_G)^{2n})^{1/2n} \quad (10)$$

In Eq. (10), if $n = 1$, the interactive slenderness ratio $\lambda_{I,1}$ is given by

$$\lambda_{I,1} = \lambda_L \lambda_G \sqrt{\left(\frac{1}{\lambda_L}\right)^2 + \left(\frac{1}{\lambda_G}\right)^2} \quad (11)$$

where λ_L and λ_G are the local and global slenderness ratios, respectively, determined as follows (Sause and Braxtan 2011)

$$\lambda_L = \sqrt{\frac{\tau_y}{\tau_{L,el}}} \quad (12)$$

where $\tau_{L,el}$ is given in Eq. (1) where $k_L = 5.34$ is used, and

$$\lambda_G = \sqrt{\frac{\tau_y}{\tau_{G,el}}} \quad (13)$$

where $\tau_{G,el}$ is given in Eqs. (5) and (6) where $k_G = 31.6$ is used.

Even though the original model by Barakat *et al*. (2015) predicts results close to the test results, it overestimates the shear strength for values of interactive slenderness ratios less than 0.75. In addition, from a design point of view, the model is considered under-conservative. For these reasons, in this paper, a new model, ρ_{S2}, is proposed, and is given in the following general form

$$\rho_{S2} = \frac{a}{\lambda_{I,2}^m} \leq 1 \quad (14)$$

where a and m are constants to be determined and $\lambda_{I,2}$ is given by Eq. (10) with $n = 2$.

Fig. 3 illustrates the effect of varying a and m on the normalized strength. Clearly, a controls the length of the plateau segment of ρ_{S2} curve while m controls the second segment (i.e., the curved segment). For a fixed value of m, increasing the parameter a lengthens the plateau segment of the curve. And for a fixed value of a, increasing m sharpens the transition between the two segments of the curve and increases the curvature of the second segment while maintaining the length of the plateau segment.

The general form of the proposed model is flexible as it can be used to describe the behavior of many buckling phenomena. One way to control the shape of the curve is to

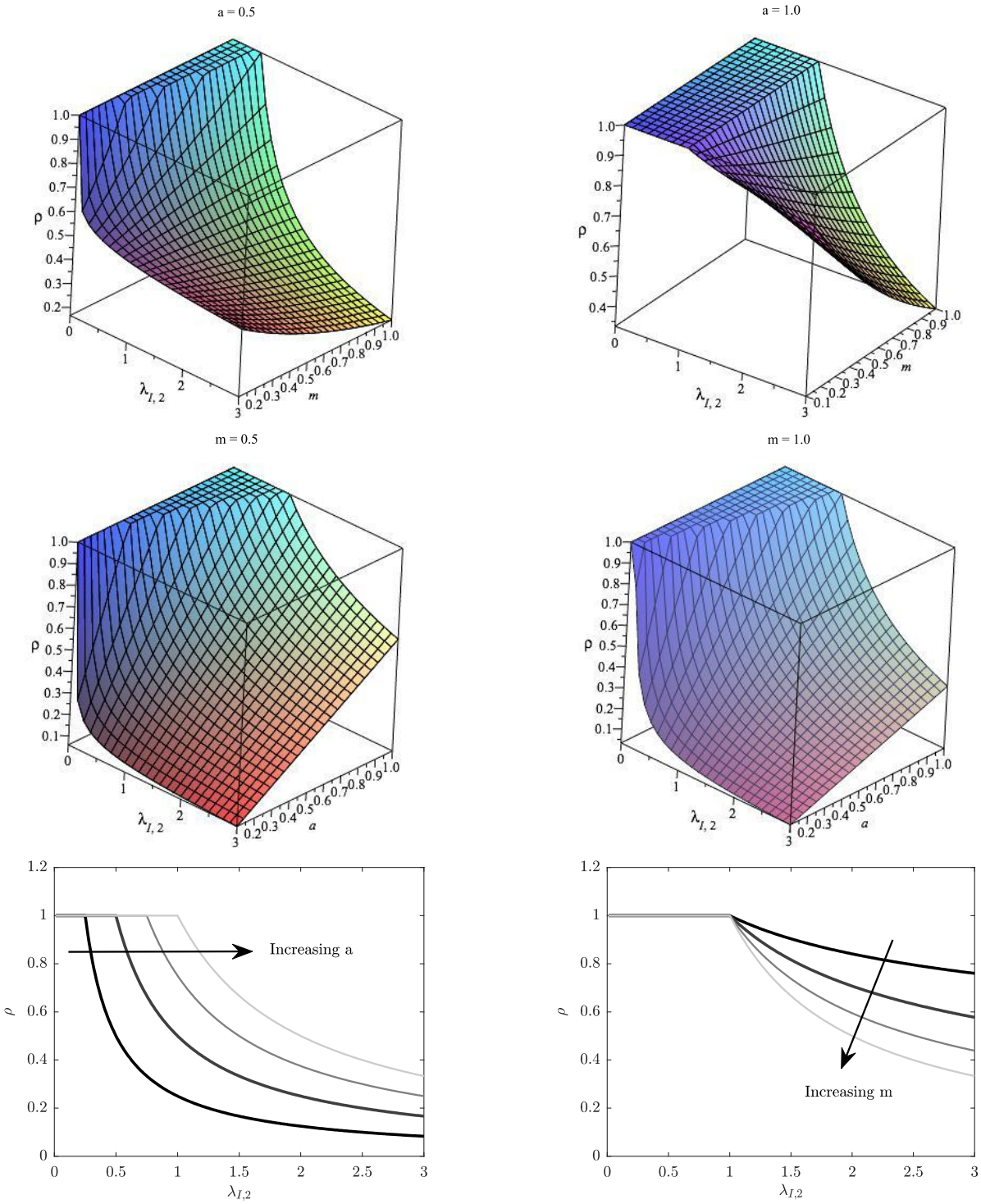

Fig. 3 Effect of varying a and m on the normalized strength of Eq. (14)

locate the value of the slenderness ratio, λ_{50}, at which $\rho_{S2} = 0.5$, which can be easily calculated to be

$$\lambda_{50} = (2a)^{\frac{1}{m}} \tag{15}$$

The condition $\lambda_{I,2}^{m} < a$ (Eq. (14)) is set to ensure a smooth transition between the two parts of the piecewise equation. To obtain an accurate estimate of the normalized shear strength, yet conservative enough for design purposes, the following constrained optimization problem is formulated and solved:

maximize the mean of $\frac{\rho_{S2}}{\rho_e}$

subjected to

$$\max\left(\frac{\rho_{S2}}{\rho_e}\right) \leq 1.15$$

$$\min\left(\frac{\rho_{S2}}{\rho_e}\right) \geq 0.55$$

$$\%\ \text{of closest fit} \geq 15\ \%$$

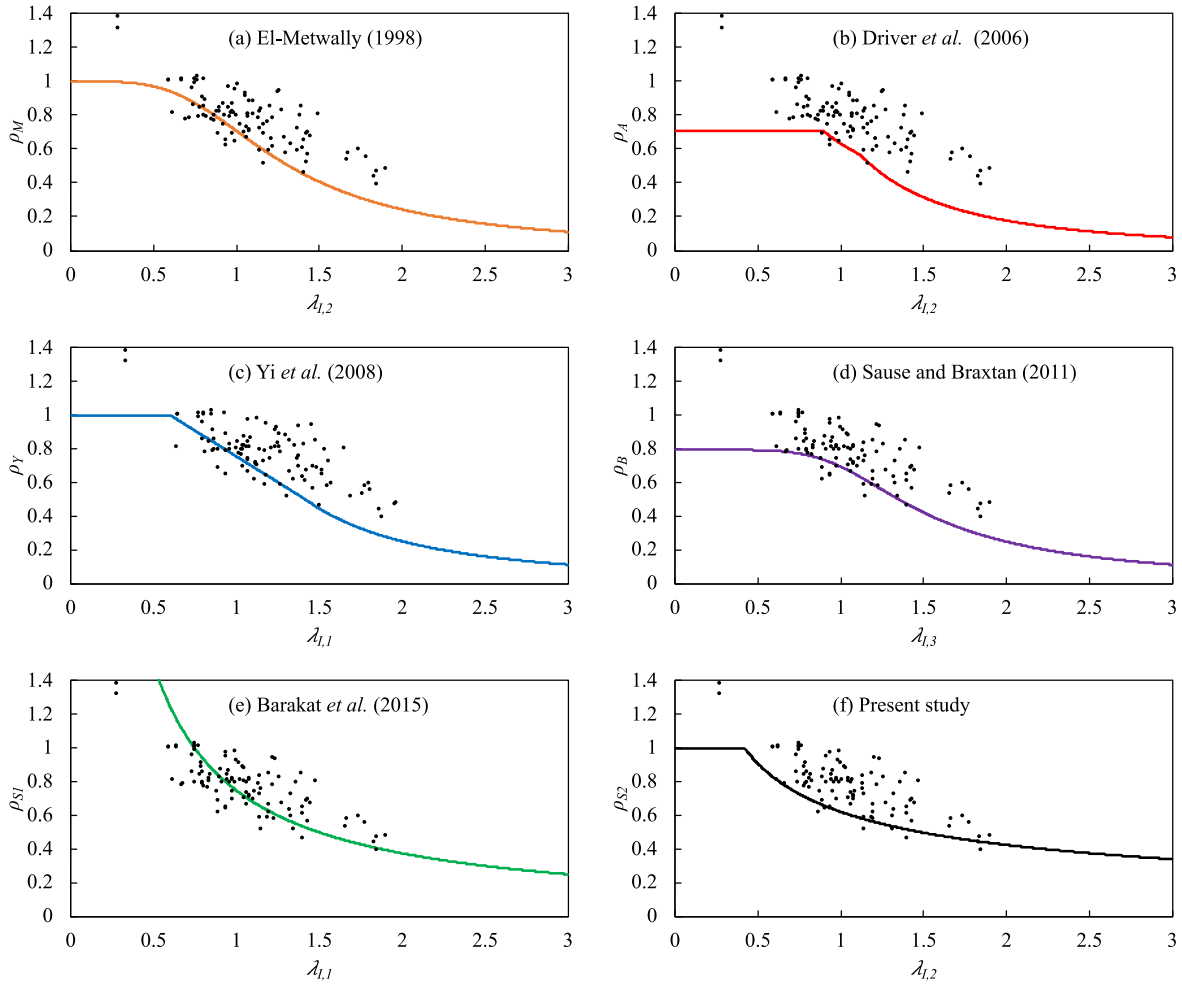

Fig. 4 Comparison of predicted normalized shear strength with test data

Table 1 Statistical comparison between the prediction models

Model	Max $(\boldsymbol{\rho/\rho_e})$	Min $(\boldsymbol{\rho/\rho_e})$	% closest fits	% $\boldsymbol{\rho > \rho_e}$	Mean $\boldsymbol{\rho/\rho_e}$	Std.	CoV
El-Metwally (1998)	1.21	0.51	22.55	17.65	0.85	0.17	19.66
Driver *et al*. (2006)	1.18	0.51	14.71	6.86	0.80	0.14	17.78
Yi *et al*. (2008)	1.22	0.45	19.61	16.67	0.83	0.18	21.17
Sause and Braxtan (2011)	1.20	0.54	22.55	9.80	0.83	0.15	17.54
Barakat *et al*. (2015)	1.67	0.55	21.57	22.55	0.89	0.19	21.99
Present	1.14	0.58	16.67	4.90	0.81	0.12	14.14

The % of closest fit is calculated as the number of accurately predicted tests over the total number of tests. Accuracy of the prediction is assumed if $0.9 \leq \rho_{S2}/\rho_e \leq 1$. The choice of the target limits in the above optimization problem is based on the observed performance of existing models, the limitations of the two-parameter proposed model itself, and the variability in the available test data. Using SOLVER in Excel® to solve the above optimization problem yielded the values $a = 0.62$ and $m = 0.55$.

Fig. 4 compares the proposed model, ρ_{S2}, model by Barakat *et al*. (2015), ρ_{S1}, Sause and Braxtan model (2011), ρ_B, Yi *et al*. model (2008), ρ_Y, Driver *et al*. model (2006), ρ_A, and El-Metwally model (1998), ρ_M, against experimental data. The set of experimental data comprises all the 102 tests collected by Sause and Braxtan (2011). From the figure, we observe first that all models underestimate the experimental normalized shear strength, $\rho_e = \tau_e/\tau_y$. However, the models by Driver *et al*. (2006) and Sause and Braxton model (S&B) (2011) are too conservative compared to the rest of the models. Statistics of the ratio $\rho_{\text{model}}/\rho_e$ for all models are illustrated in Table 1 and in the boxplots and whiskers shown in Fig. 5. It is clear that the proposed model predictions are contained in a narrow range, [0.58, 1.14], while the other models have predictions in larger ranges, from 0.45 to 1.67. The mean values estimated by all models are in the range [0.81-0.89],

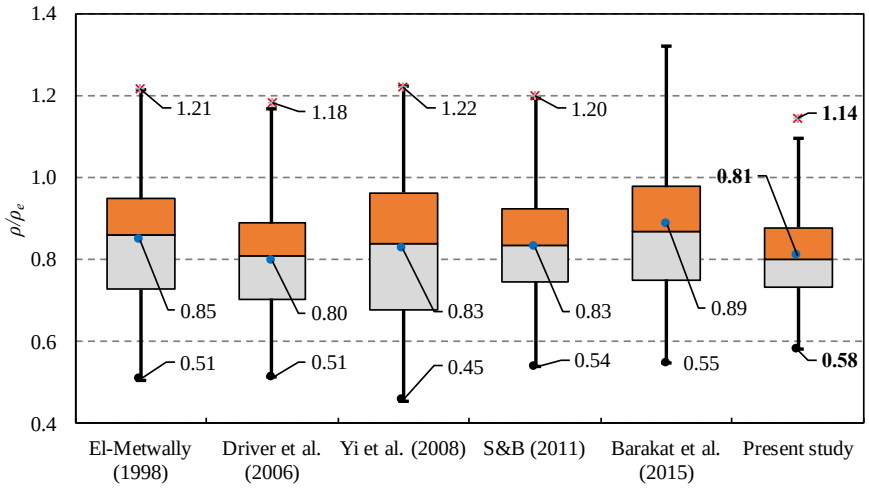

Fig. 5 Boxplots and whiskers for ρ/ρ_e by different models

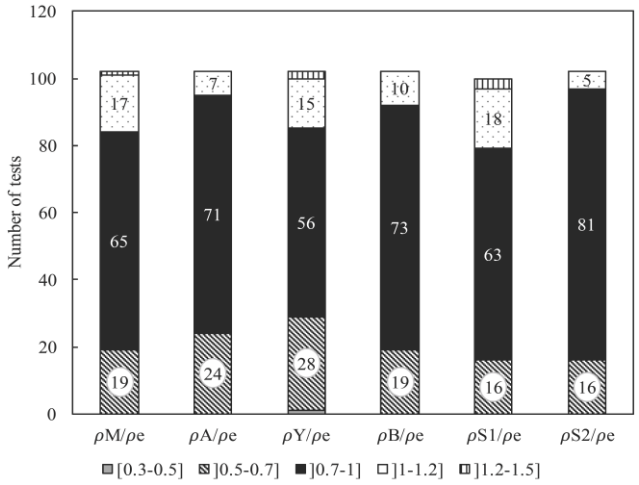

Fig. 6 Number of tests with ρ/ρ_e ratios falling in different ranges

Fig. 7 View of an actual beam specimen

suggesting an underestimation of the experimental shear strength by about 11-19%. The maximum and minimum ρ/ρ_e indicate how well the analytical models are performing for the whole test database. Barakat *et al*. model predictions have the highest mean ($\rho_{S1}/\rho_e = 0.85$), followed by El-Metwally's model (1998) ($\rho_M/\rho_e = 0.85$), the models by Sause and Braxtan (2011) and Yi *et al*. (2008), which have an equal mean of 0.83, then the present model ($\rho_{S2}/\rho_e = 0.81$), and finally the model by Driver *et al*. (2006) ($\rho_A/\rho_e = 0.80$). However, predictions by all previously published models have a higher variability, thus higher dispersion, as evidenced by their coefficients of variation, CoV, (taking values from 17.54% to 22% of the mean) and by their interquartile ranges, IQR, (taking values from 0.18 and 0.22). The CoV for the proposed model is 14.14% of the mean ρ_{S2}/ρ_e and the IQR is 0.15, suggesting a lower dispersion of its predictions. In addition, the boxplots corresponding to both, the present and Sause and Braxtan models are symmetric, whereas the rest of the predictions are negatively skewed.

Fig. 6 shows the number of tests with ρ/ρ_e falling in five ranges. The figure demonstrates quantitatively to which level the predictive models tend to be conservative. For instance, the proposed model predicts accurately (ρ/ρ_e in the range [0.7-1.0]) 81 out of the 102 test results (i.e., 79.4%), which is the largest quantity among all models. However, it underestimates ($\rho_{\text{model}}/\rho_e < 0.7$) 16 test results and overestimates only 5 tests (($\rho_{\text{model}}/\rho_e > 1$)), which are the smallest quantities across all previously published models.

The proposed ρ_{S2} model presents a compromise between accuracy and conservatism for both economic and design purposes. As mentioned earlier, ρ_B model by Sause and Braxton was validated for 22 tests only. However, this analysis doesn't suggest that the other models are not limited in applicability.

3. Experimental program

3.1 Test setup

Six corrugated web steel beams were fabricated in a local workshop. The beams are composed of two 150 mm wide and 12 mm-thick flanges and a trapezoidal corrugated steel web (Fig. 7). Six 12 mm-thick stiffeners were added to the beams as shown in Fig. 7. The mechanical properties of the material were determined based on three coupon specimens subjected to uniaxial tensile tests. The elastic

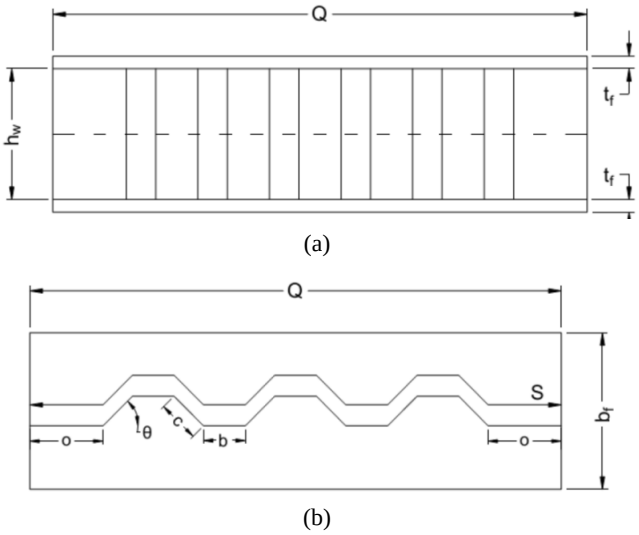

Fig. 8 Geometric parameters of beam specimens

Table 2 Dimensions of test beams

#	Specimen	h_w (mm)	θ (°)	Q (mm)	a/h_w
1	B12-305-30	305	30	996	1.40
2	B12-305-45	305	45	920	1.28
3	B12-410-30	410	30	996	1.04
4	B12-410-45	410	45	920	0.95
5	B12-505-30	505	30	996	0.85
6	B12-505-45	505	45	920	0.77

modulus of the steel material was determined to be 200 GPa and the yield strength to be 230 MPa. Three different depths (h_w), one thickness (t_w = 1.2 mm), and two different angles of corrugation (θ) were used for the webs, resulting in a total of six ($3 \times 1 \times 2$) different combinations (see Fig. 8). The dimensions of the beams are listed in Table 2.

With reference to Fig. 8 and Table 2, the other geometric parameters of the beams were fixed as: $b = c =$ 40 mm, and $o =$ 70 mm. Each web was welded to the flanges using a combination of continuous and intermittent welding. At the top of the beam, one side was welded continuously while the opposite was welded only at the interface between the longitudinal folds of the web and the flange. At the bottom of the beam, the same pattern was repeated in reverse. The result was that the top, bottom, and both sides of the web, each had one edge continuously welded and one edge intermittently welded. Fig. 9 shows the welding locations on a sample beam. This technique ensures a strong bond between the web and flanges while distributing the strength of the bond as evenly as possible.

Fig. 10 shows the experimental setup. The beams were simply supported and loaded at the center. An overhang of 70 mm past each support was provided to prevent the beams from slipping off the supports during testing. For each bean, a total of four strain gauges (SGs) were installed, two on either side of every beam at a quarter-span from the supports. To measure the deflection of the beam, three linear variable differential transformers (LVDTs) were

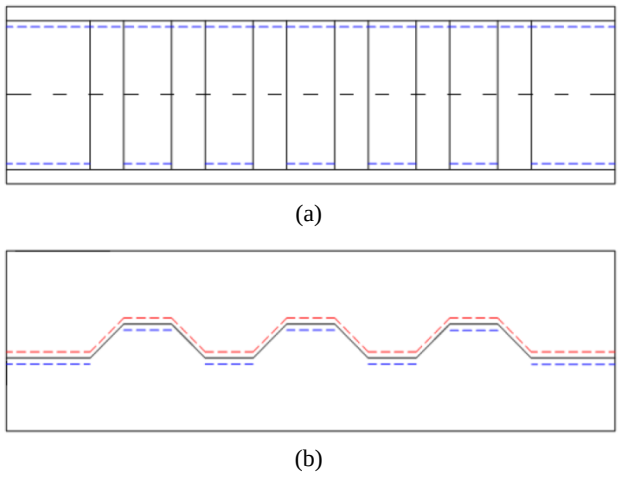

Fig. 9 Welding locations highlighted in dashed lines

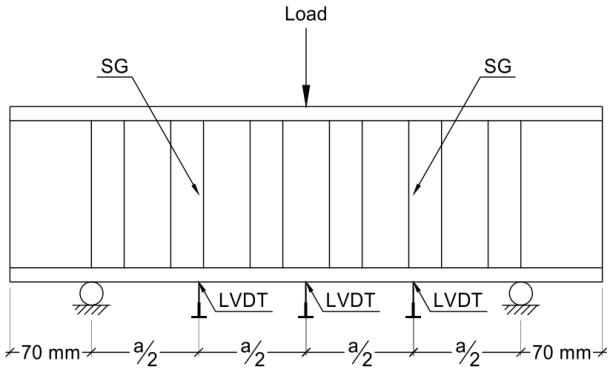

Fig. 10 Loading setup and locations of strain gauges and LVDTs

installed underneath each beam prior to testing at the locations indicated in the same figure.

The beams were tested under displacement control at a rate of 0.02 mm/s. The load applied by the actuator was monitored continuously. The testing was stopped after the load had dropped significantly after the web was observed to have buckled.

3.2 Results and discussion

Table 3 summarizes the experimental shear capacities obtained from the static tests of all six beams. Figs. 11-16 show the load-mid span deflection curves along with the status of the beam at various loading stages (marked from

Table 3 Experimental shear capacities of tested beams

#	Specimen	Experimental shear capacity V_e (kN)
1	B12-305-30	53.43
2	B12-305-45	51.77
3	B12-410-30	66.31
4	B12-410-45	73.14
5	B12-505-30	80.98
6	B12-505-45	87.85

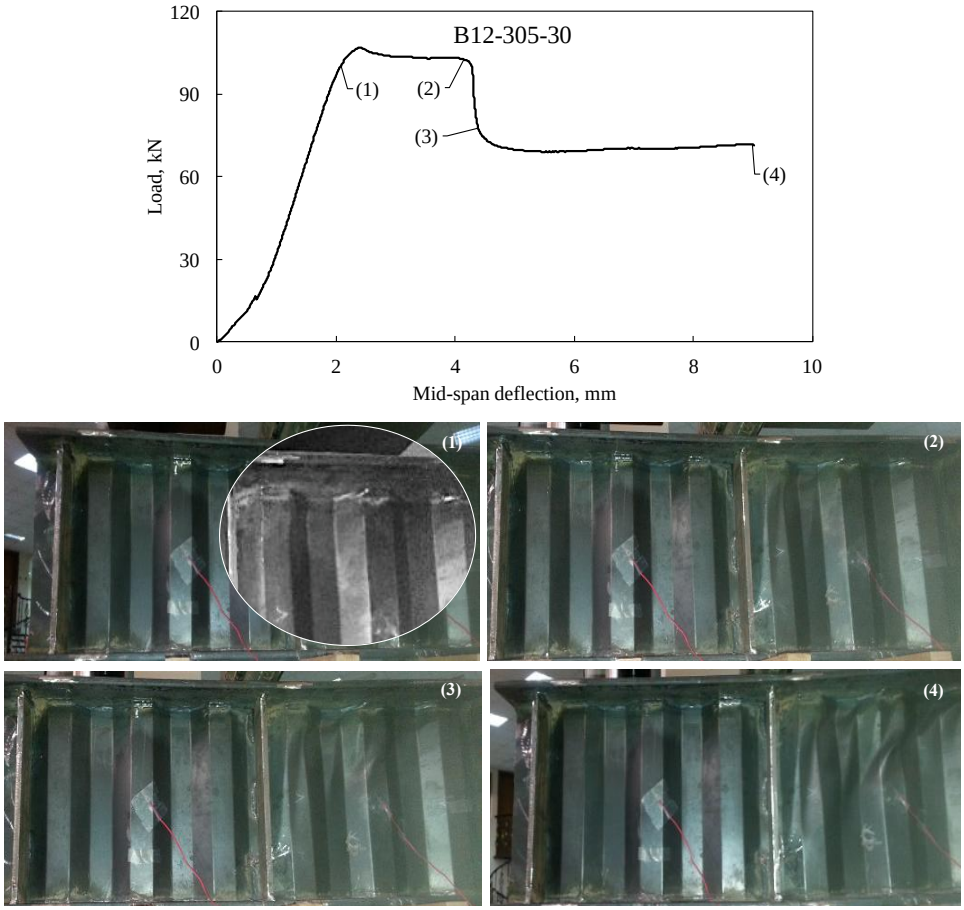

Fig. 11 Load versus mid-span deflection curve for specimen B12-305-30

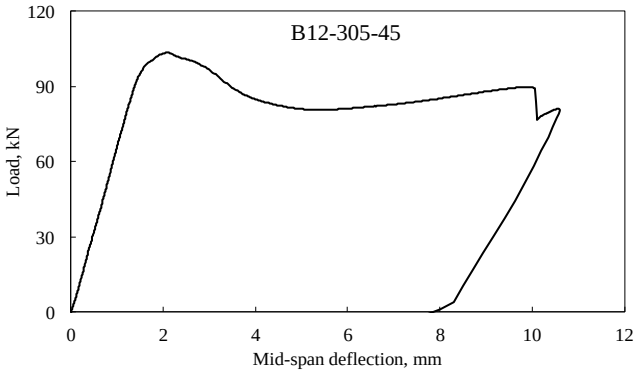

Fig. 12 Load versus mid-span deflection curve for specimen B12-305-45

1 to 4). Fig. 17 shows images of the beams at the end of tests. Fig. 18 shows the load-strain curves as recorded by the four strain gauges. The strain at the onset of buckling, ε_e, was normalized by the yield strain, ε_y, and reported in Table 4. The following discussion will be made with reference to Figs. 11-18 and Tables 3-4.

Beam B12-305-30, which features a web depth of 305 mm and angle of corrugation of 30°, failed due to shear buckling at a load level of 106.9 kN, which is equivalent to a shear load of 53.4 kN. An image of the mode of failure is shown in (Fig. 17(a)) and the load versus mid-span deflection curve along with for this beam is shown in Fig. 11.

At the buckling stage (load stage 1 as illustrated in Fig. 11), a bulge appeared at the top of the longitudinal fold #1, which is the closest to the middle stiffener. As the beam is pushed further (stage 2), a steep wave developed at the location of the initial bulge and extending to the center of the beam till the bottom flange. In addition, a small bulge appeared at the right of the previous wave. Right after this stage, the load dropped instantaneously by 35% (stage 3) and the new bulge developed into a crease extending diagonally from the top of the right stiffener down the mid-height of the right web panel. The test was terminated (stage 4) after no further difference was noticeable on the shape of the beam nor on the load-deflection curve.

The mode of failure of the web was interactive close to local since it started at the longitudinal folds, which extended to adjacent longitudinal folds and the diagonal folds were not under excessive out-of-plane deformations, until the end of test (Fig. 17(b)).

Specimen B12-305-45 (Fig. 12), which differs from the previous beam by the angle of corrugation, failed due to interactive shear buckling at a load of 103.5 kN, which is equivalent to a shear load of 51.8 kN. By the end of the test, three large wrinkles had formed and propagated to cover half of the web's depth. Before load removal, the beam had reached a residual strength of about 78% of the shear buckling load. After load removal, the beam showed

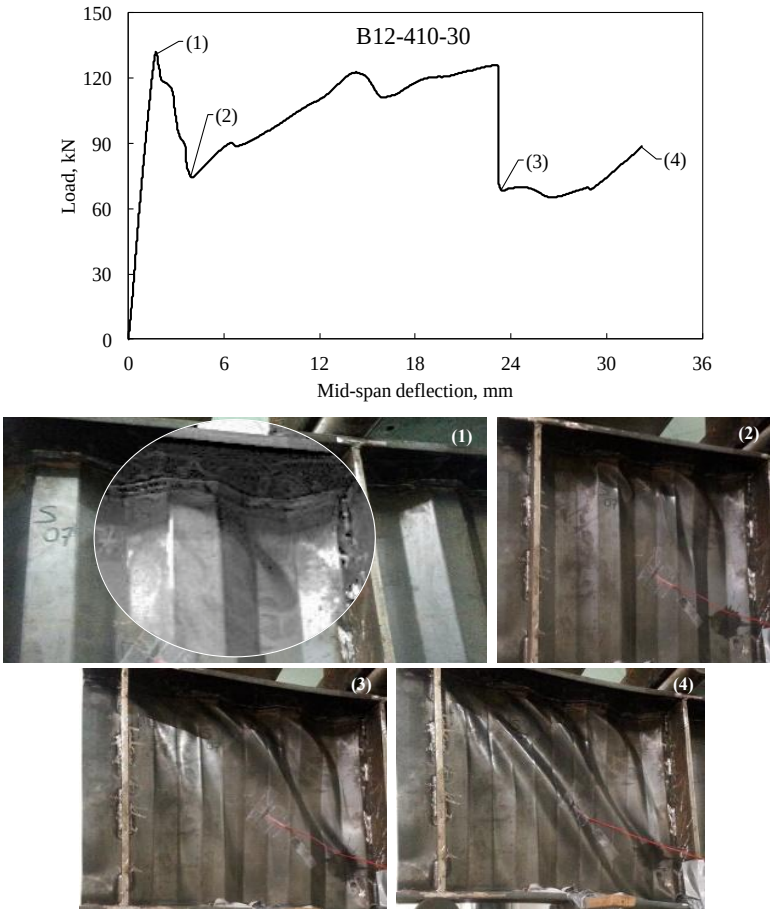

Fig. 13 Load versus mid-span deflection curve for specimen B12-410-30

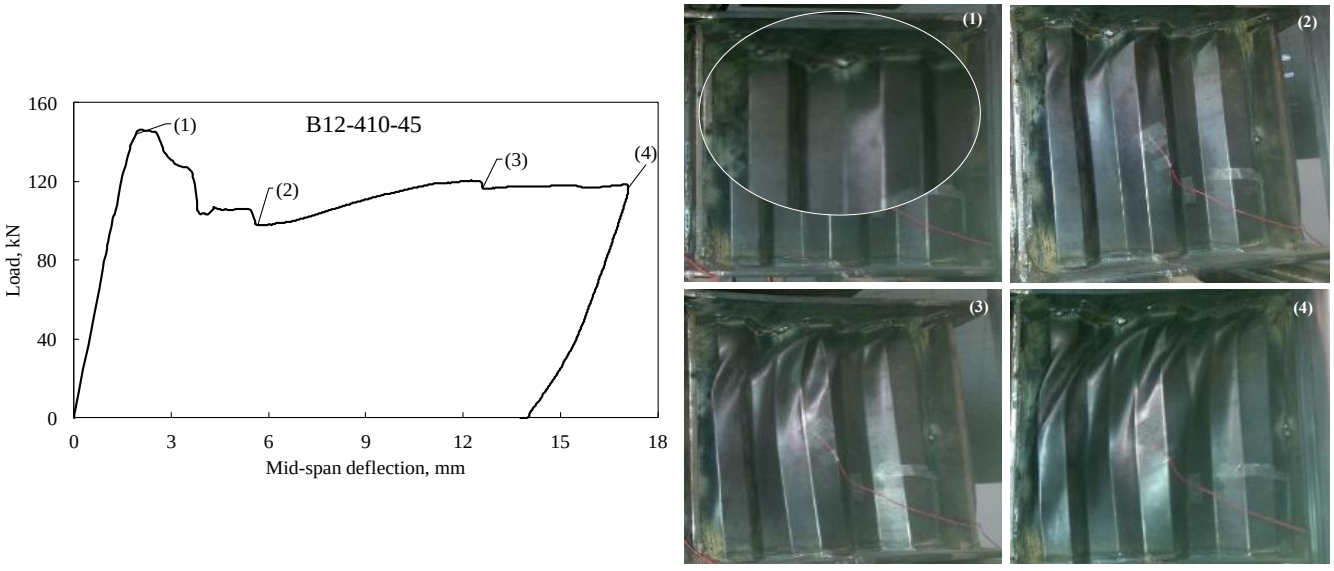

Fig. 14 Load versus mid-span deflection curve for specimen B12-410-45

a permanent central deflection of 8 mm (Fig. 17).

Beam B12-410-30, which differs from the first beam (i.e., B12-305-30) by the web depth ($h_w = 410$ mm in the current beam), failed due to shear buckling at a shear load of 66.31 kN. The appearance of the beam after failure is shown in Fig. 17(c) and the load versus mid-span deflection curve is shown in Fig. 13.

With reference to Fig. 13, at the onset of buckling (stage 1) small bulges appeared at the top of the longitudinal and diagonal folds of the left web panel, close to the middle stiffener. Afterwards, the load instantaneously dropped, and the bulges developed into two main creases covering almost

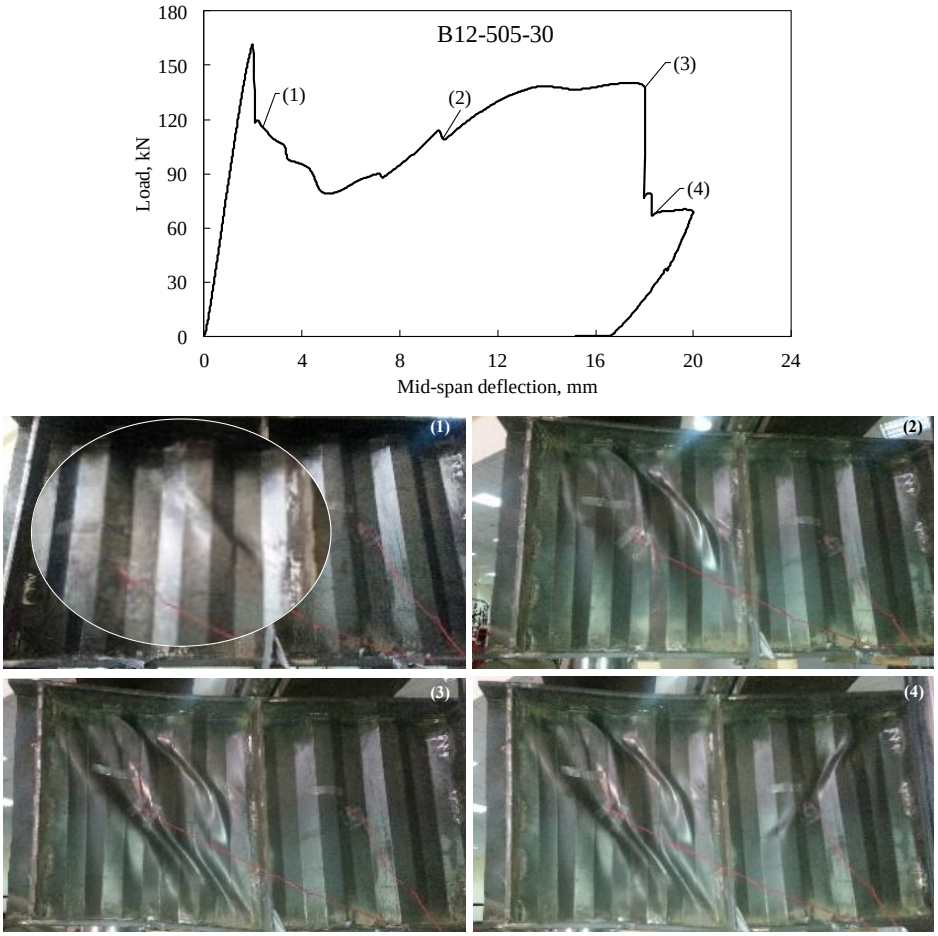

Fig. 15 Load versus mid-span deflection curve for specimen B12-505-30

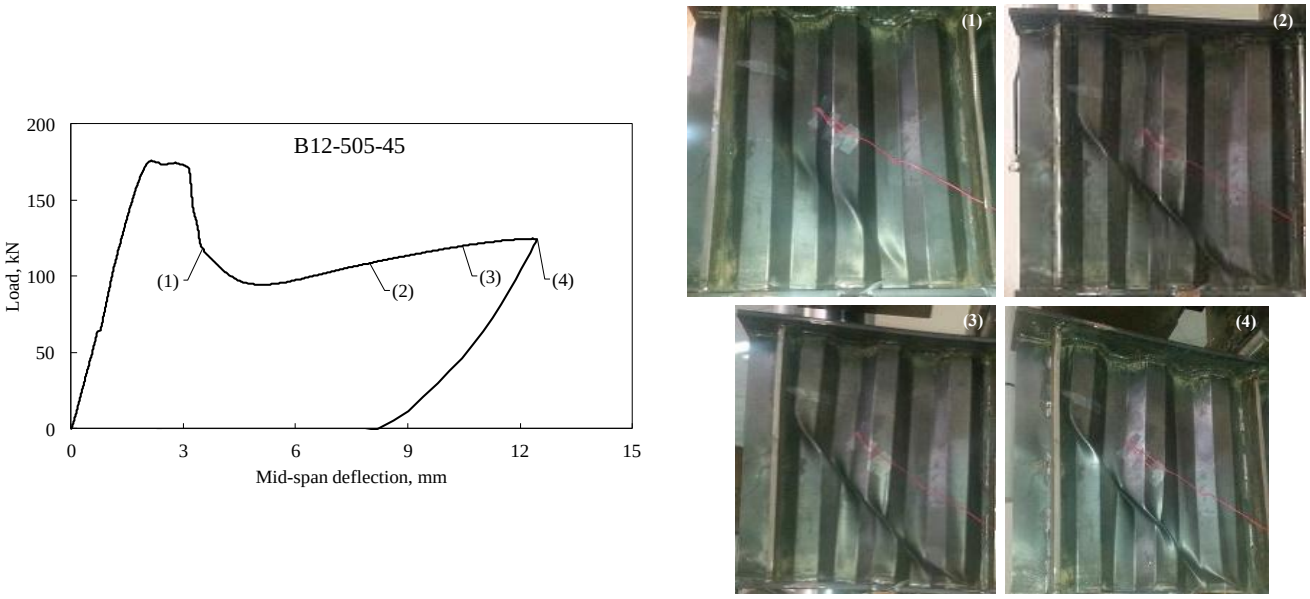

Fig. 16 Load versus mid-span deflection curve for specimen B12-505-45

the top half of the left web panel. Before the end of stage 2, two creases, symmetric to the previous ones, appeared on the right side of the beam, close to the middle stiffener. Immediately after load stage 2, the beam picked-up 95% of its load bearing capacity, then again dropped it instantaneously when pushed down further (stage 3). At this stage, the previously formed creases continued to gain more depth and propagated further to cover almost ¾ of the web

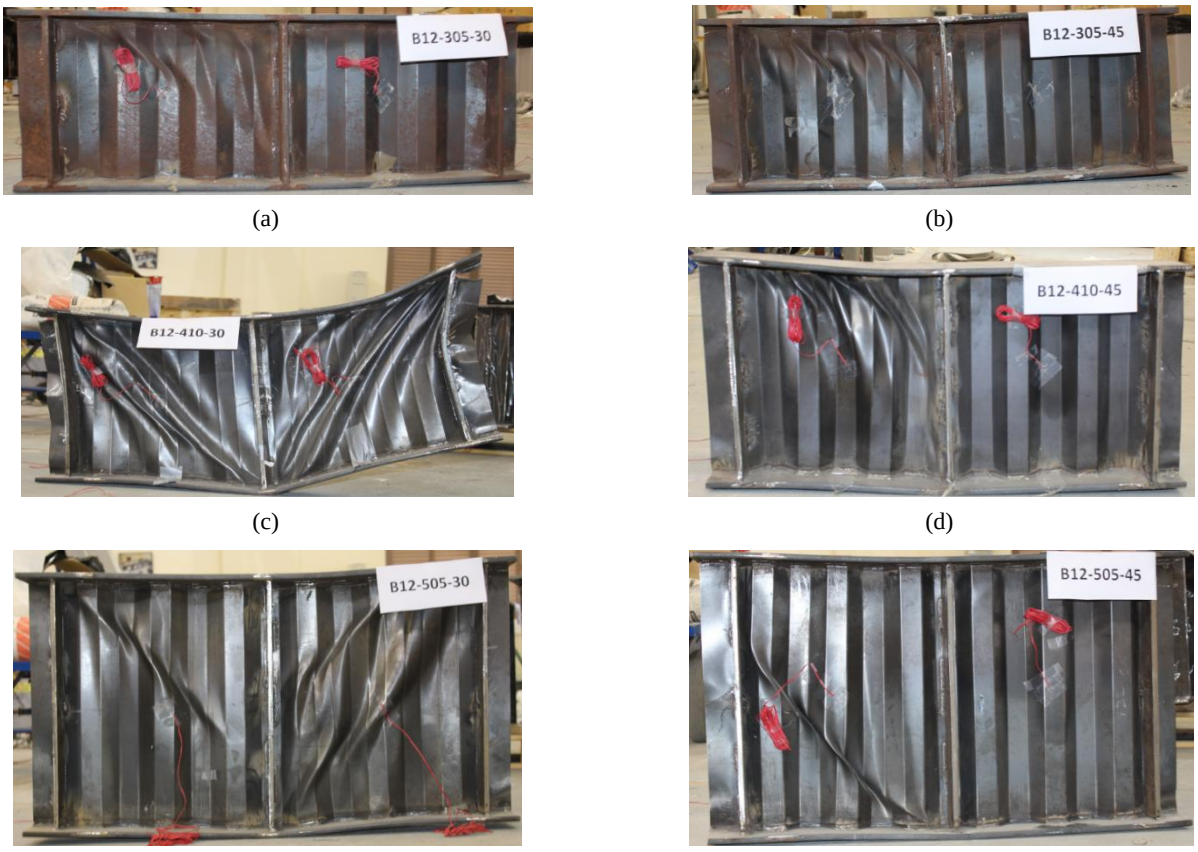

(a) (b) (c) (d) (e) (f)

Fig. 17 Failure modes of tested beam specimens

depth. In addition, more wrinkles appeared on top of both sides of the beam, near the support stiffeners. Pushing further the beam resulted in an increase of its load bearing capacity to reach 70% of its buckling load (stage 4). The beam failed to carry more load after this stage, and all creases and wrinkles developed into diagonal waves covering the entire web panels. It should be noted this beam recorded a residual strength of more than 90 kN (i.e., 68% of the ultimate load).

By analyzing the load-deflection curve, each of the peak and dale pairs correspond to the development of interactive mode of buckling; as the beam is pushed and the load increases, the buckle extends diagonally (peak) until the next buckle appears in another fold, followed by a decrease of the load bearing capacity (dale).

Similarly, the beam B12-410-45, which is different than the previously discussed beam (i.e., B12-410-30) only in terms of the corrugation angle (45° in the current beam), as shown in Fig. 14, buckled due to an interactive shear buckling as evidenced by the formation of bulges in the diagonal (inclined) folds #3 and #5 of the right half of the web. The buckling occurred at a load of 146.28 kN, which is equivalent to a shear load of 73.1 kN. The sequence of images shown in Fig. 14 clearly relate the drop in load carrying capacity of the web with the formation of wrinkles, in the form of staircase steps; the number of steps corresponds to the number of wrinkles appearing in the web as the load increases. After multiple wrinkles had formed, the beam ultimately failed at a load of 116 kN, which is equivalent to a residual strength of about 80% of the shear buckling load. After load removal, the beam showed a permanent central deflection of 14 mm (Fig. 17(d)).

Beam B12-505-30, which is deeper version to B12-410-30 ($h_w = 505$ mm in the current beam), failed due to shear buckling at a shear load of 81 kN. The appearance of the beam after failure is shown in Fig. 17(e) and the load versus mid-span deflection curve is shown in Fig. 15.

With reference to Fig. 15, at the onset of buckling (stage 1) small bulges appeared at the top of the longitudinal and diagonal folds of the left web panel, close to the middle stiffener. Afterwards, the load instantaneously dropped, and the bulges developed into three main creases covering almost the top half of the left web panel. At load stage 3, the beam picked-up its load bearing capacity, however, a new bulge appeared at the top of the right web panel, indicating that this panel is responsible for the increase of the beam's overall bearing capacity (from 108.84 kN at load stage 2 to 139.478 kN at load stage 3). The beam failed to carry more load at this stage and the bulge that appeared on the left web panel, now, has developed into a diagonal crease (stage 4). Prior to its ultimate failure, the beam continued to carry loads well beyond the buckling stage, recording a residual strength of about 50% of the ultimate load.

Similar to B12-410-30, the load-deflection curve shows multiple pairs of peaks and dales, corresponding to an interactive shear buckling mode of failure (Fig. 17(e)).

A total different behavior was observed in beam B12-505-45. The only difference between this beam and the

previous one (i.e., B12-505-30) is the corrugation angle only (45° in the current beam versus 30° in the previous one). At buckling (stage 1), bulges appeared in the longitudinal and diagonal folds (subpanels) at the left web panel, below the location of SG2. These bulges developed quickly (stage 2) into a single wrinkle as shown in Fig. 16. At load stage 4, the beam reached its ultimate load bearing capacity, hence the test was terminated immediately. Note that by the end of the test, a tiny bulge appeared at the top of the right web panel, close to the middle stiffener. The failure occurred due to interactive shear buckling at a load of 175.7 kN, which corresponds to a shear buckling load of 87.85 kN (Fig. 16). The residual strength in the beam reached 70% of the load carrying capacity. The appearance

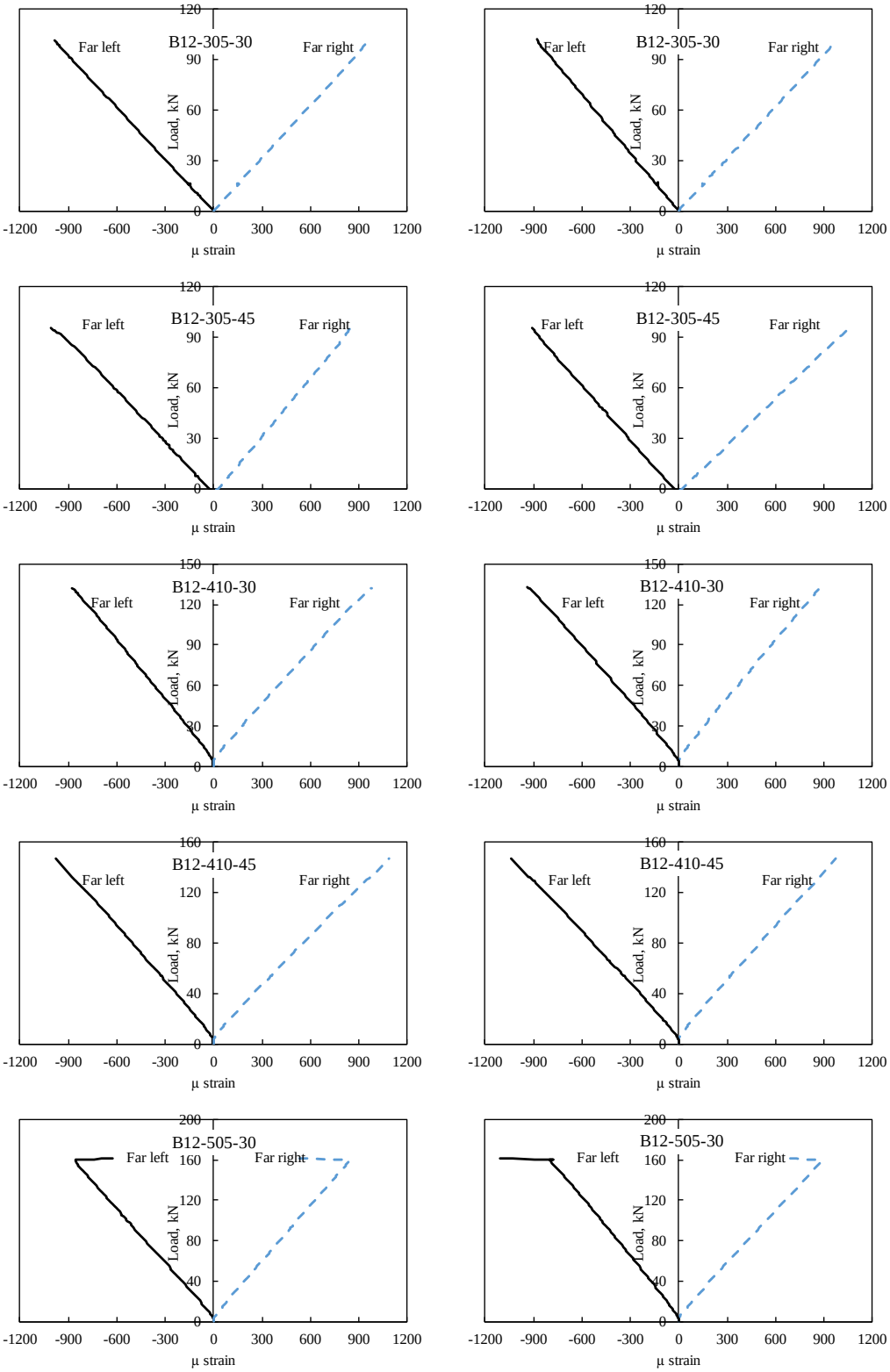

Fig. 18 Load-strain curves

Table 4 Comparison of yield strain with experimental strain

Specimen	$\varepsilon_e/\varepsilon_y$			
	Near right*	Near left*	Far right†	Far left†
B12-305-30	-0.80	0.90	0.86	-0.91
B12-305-45	-0.88	0.74	0.94	-0.79
B12-410-30	-0.85	0.86	0.76	-0.82
B12-410-45	-0.85	0.83	0.9	-0.85
B12-505-30	-0.54	0.57	0.42	-0.97
B12-505-45	-0.91	0.92	0.87	-0.93
Average $\mu\varepsilon_e/\mu\varepsilon_y$	-0.81	0.80	0.79	-0.88

* Near right and near left refer to the strain gauges located on the front side of the beam

† Far right and far left refer to the strain gauges located on the back side of the beam

of the beam after failure is shown in (Fig. 17(f)).

A study of the load-strain curves (Fig. 18) reveals that the beams buckled before the yield strain (ε_y =1150 μ-strains) for the web's material is reached. The graphs show the strain measured on either side of the buckled panel of the corresponding beam. Table 4 lists the normalized experimental strains ($\varepsilon_e/\varepsilon_y$) that correspond to the peak load for each beam. For all beam specimens, the average strain measured at the point of buckling is less than the yield strain ($\varepsilon_e/\varepsilon_y$ = 0.77-0.86). This suggests a geometric rather than material failure. However, the design of the beams almost takes full advantage of the strength of the material (e.g., 97% of the material strength in beam B12-505-30). In addition, the beams with 45° corrugations reached a higher strain at the point of buckling than those with 30° corrugations. This indicates that 45° corrugations performed better than 30° corrugations. The lower ratios reported for the B12-505-30 were due to the early debonding caused by the deep wrinkles that appeared on the faces of the web where the strain gauges are attached.

4. Comparison of proposed and previous models with test data

Table 5 compares the experimental shear capacities, V_e, of all tested beams, with the shear capacities predicted using the current, V_{s2} and previously proposed models (by Barakat *et al*. (2015), V_{S1}, Sause and Braxtan model (2011), V_B, Yi *et al*. model (2008), V_Y, Driver *et al*. model (2006), V_A, and El-Metwally model (1998), V_M).

Results of the proposed model (V_{s2}) and those of the models (V_Y) and (V_M) are closer to the test results than the results of the models (V_B) and (V_A); the former models have an average predicted-to-experimental shear capacity ratio (V_{model}/V_e) of 0.87, 0.93 and 0.91, respectively, whereas the latter's are 0.74 and 0.66, respectively. Fig. 19, compares the prediction of various models with experimental results. The results indicate that all predictions are dispersed away from the equality line but in the conservative side, except V_{S1}.The V_{S1}model overestimated the shear strength of all specimens since their normalized slenderness ratios are below 0.75. Again, this is one of the main reasons why V_{S2} model is proposed as a modification to V_{S1} model. For this set of tests, the predictions of V_Y, V_M, and V_{S2} models are closer to the equality line in a descending order indicating that V_Y and V_M models are the best fit models. However, as explained earlier, this is not the case when considering the whole tests in the database. On the other hand, V_A and V_B models are considered conservative predictions for all specimens that might lead to uneconomical designs.

It should be noted that three of the tested beams fall within the limits set by Sause and Braxton (2011) in the development of their model ($a/h_w > 1$, $\theta \geq 22°$, $0.87 \leq \beta \leq 1.13$) (see Table 1), whereas the proposed model is meant to give consistent results for wider ranges and larger combinations. Considering the dispersion, accuracy, consistency and economical aspects of the prediction models, the authors recommend their proposed model over the rest of the models.

5. Conclusions

This paper presents experimental and analytical studies on the shear buckling behavior of corrugated web steel beams (CWSBs). First presented are the commonly known existing analytical models for the estimation of shear bucking of CWSBs, which include the models by El-Metwally (1998), Driver *et al*. (2006), Yi *et al*. (2008), Sause and Braxtan (2011), and Barakat *et al*. (2015). The performance of these models is assessed against a database of 102 experimental test results with various corrugation configurations and geometric dimensions. The results of this comparison showed large scatters between the

Table 5 Comparison of test and predicted results (unit: kN)

Specimen	V_e	V_M/V_e	V_A/V_e	V_Y/V_e	V_B/V_e	V_{S1}/V_e	V_{S2}/V_e
B12-305-30	53.43	0.89	0.64	0.91	0.72	1.30	0.88
B12-305-45	51.77	0.93	0.66	0.94	0.74	1.49	0.94
B12-410-30	66.31	0.95	0.70	0.98	0.78	1.21	0.88
B12-410-45	73.14	0.88	0.63	0.89	0.71	1.27	0.87
B12-505-30	80.98	0.93	0.70	0.94	0.78	1.07	0.81
B12-505-45	87.85	0.89	0.65	0.92	0.73	1.17	0.84
	Average	0.91	0.66	0.93	0.74	1.25	0.87

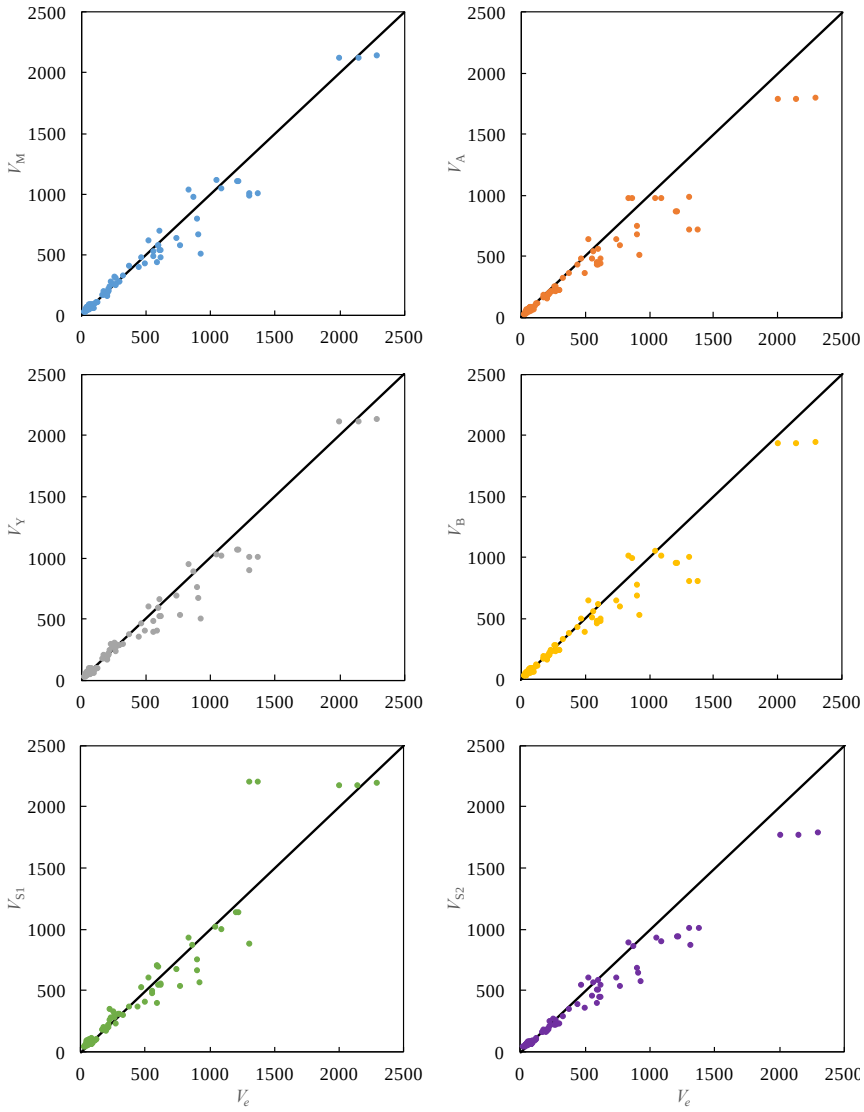

Fig. 19 Comparison of test and predicted results

prediction of considered models and the experimental values. In addition, none of these models predict the CWSB shear capacity very accurately nor conservatively, which is of serious concern considering any of the models in the design of such beams. To address both accuracy of prediction and economic design concerns, the previously published model by Barakat *et al*. (2015) was modified based on an optimization formulation with certain constraints obtained by analyzing the existing test database and the prediction of existing models.

Next, six shear-critical CWSBs with three different depths (h_w), one thickness (t_w), and two different corrugation angles (θ) are fabricated and tested under three-point load in a displacement control test setup until failure. Two modes of failure are observed across all beams, local and interactive shear buckling. The new experimental results are used to update the existing database for further comparisons. Finally, the paper looks at the adaptability of the prediction models (existing and proposed) on the updated results database. Based on the results of this research, one can draw the following conclusions:

(1) In terms of performance and given the wide scatter in the available database, not all existing prediction models give accurate or conservative results and therefore cannot be used for design purposes. Among all models studied, the proposed model gave accurate results for 80% of the tests, while 16% are underestimated and only 4% overestimated, which is significantly better than all other studied models.
(2) The residual strength in all currently tested beams is high and varies from 50 to 80% of the buckling load.
(3) The experimental results indicate that the tested corrugated web beams consume an average of 77-86% of the material strength before failure. Even though this suggests a geometric rather than material failure, still, the material strength is utilized to a high degree by all CWSBs.
(4) CWSBs with 45° corrugations reached higher strain levels at failure when compared with 30° corrugation CWSBs. This indicates that beams with

45° corrugations utilize the material strength to a higher degree of effectiveness and therefore offer a more efficient design alternative.

(5) Considering the dispersion of test data, accuracy, consistency, and economical aspects of the prediction models, the proposed model in this study is recommended by the authors for the design of CWSBs over the rest of the models.

Acknowledgments

This work was supported by a competitive grant (1502040112-P) from the University of Sharjah and by the Sustainable Construction Materials and Structural Systems (SCMASS) research group, University of Sharjah. This support is highly acknowledged.

References

Abbas, H.H. (2003), "Analysis and design of corrugated web I-girders for bridges using high performance steel", Ph.D. Dissertation; Lehigh University, Bethlehem, PA, USA.

Aggarwal, K., Wu, S. and Papangelis, J. (2018), "Finite element analysis of local shear buckling in corrugated web beams", *Eng. Struct.*, **16**2, 37-50.

Ahmed, S.E. (2005), "Plate girders with corrugated steel webs", *Eng. J.*, **42**(1), 1-13.

Barakat, S. and Leblouba, M. (2018), *Shear Strength of Corrugated Web Steel Beams*: *Experimental and Analytical Investigation* (No. 18-02361).

Barakat, S., Mansouri, A.A. and Altoubat, S. (2015), "Shear strength of steel beams with trapezoidal corrugated webs using regression analysis", *Steel Compos. Struct., Int. J.*, **18**(3), 757-773.

Basiński, W. (2018), "Shear Buckling of Plate Girders with Corrugated Web Restrained by End Stiffeners", *Periodica Polytech. Civil Eng.*, **62**(3), 757-771. DOI: https://doi.org/10.3311/PPci.11554

Bergfelt, A. and Leiva, L. (1984), *Shear Buckling of Trapezoidally Corrugated Girders Webs*, Division of Steel and Timber Structures, Chalmers University of Technology, Gothenburg, **84**(2).

BS EN 1993-1-5:2006 - Eurocode 3 (2006), Design of steel structures-Part 1-5: General rules - Plated structural elements; CEN, United Kingdom.

Chen, X.C., Bai, Z.Z., Zeng, Y., Jiang, R.J. and Au, F.T. (2017), "Prestressed concrete bridges with corrugated steel webs: Nonlinear analysis and experimental investigation", *Steel Compos. Struct., Int. J.*, **21**(5), 1045-1067.

Driver, R.G., Abbas, H.H. and Sause, R. (2006), "Shear behavior of corrugated web bridge girders", *J. Struct. Eng.*, **132**(2), 195-203.

Dubina, D., Ungureanu, V. and Gîlia, L. (2015), "Experimental investigations of cold-formed steel beams of corrugated web and built-up section for flanges", *Thin-Wall. Struct.*, **90**, 159-170.

Easley, J.T. (1975), "Buckling formulas for corrugated metal shear diaphragms", *J. Struct. Div.-ASCE*, **101**(7), 1403-1417.

El-Metwally, A.S. (1998), "Prestressed composite girders with corrugated steel webs", MS.C. Dissertation; University of Calgary, Canada.

Elgaaly, M., Hamilton, R.W. and Seshadri, A. (1996), "Shear Strength of Beams with Corrugated Webs", *J. Struct. Eng.*, **122**(4), 390-398.

Guo, T. and Sause, R. (2014), "Analysis of local elastic shear buckling of trapezoidal corrugated steel webs", *J. Constr. Steel Res.*, **102**, 59-71.

Hassanein, M. and Kharoob, O. (2013), "Behavior of bridge girders with corrugated webs: (II) Shear strength and design", *Eng. Struct.*, **57**(December), 544-553.

Hassanein, M. and Kharoob, O. (2014), "Shear buckling behavior of tapered bridge girders with steel corrugated webs", *Eng. Struct.*, **74**(1), 157-169.

Huang, L., Hikosaka, H. and Komine, K. (2004), "Simulation of accordion effect in corrugated steel web with concrete flanges", *Comp. Struct.*, **82**(23-26), 2061-2069.

Kharoob, O. and Hassanein, M. (2015), "Linearly tapered bridge girder panels with steel corrugated webs near intermediate supports of continuous bridges", *Thin-Wall. Struct.*, **88**, 119-128.

Leblouba, M., Barakat, S., Altoubat, S., Junaid, T.M. and Maalej, M. (2017a), "Normalized shear strength of trapezoidal corrugated steel webs", *J. Constr. Steel Res.*, **136**, 75-90.

Leblouba, M., Junaid, M.T., Barakat, S., Altoubat, S. and Maalej, M. (2017b), "Shear buckling and stress distribution in trapezoidal web corrugated steel beams", *Thin-Wall. Struct.*, **113**, 13-26.

Linder, J. and Aschinger, T.R. (1988), "Grenzschubtragfähigkeit von I-Trägern mit trapezförmig profilierten Stäben", *Stahlbau*, **57**(12), 377-380.

Lindner, J. and Huang, B. (1995), "Beulwerte für trapezförmig profilierte Bleche unter Schubbeanspruchung", *Stahlbau*, **64**(2), 370-374.

Luo, R. and Edlund, B. (1996), "Shear capacity of plate girders with trapezoidally corrugated webs", *Thin-Wall. Struct.*, **26**(1), 19-44.

Lu, Y. and Ji, L. (2018), "Behavior of optimized prestressed concrete composite box-girders with Corrugated Steel Webs", *Steel Compos. Struct., Int. J.*, **26**(2), 183-196.

Ma, Y., Ni, Y.S., Xu, D. and Li, J.K. (2017), "Space grid analysis method in modelling shear lag of cable-stayed bridge with corrugated steel webs", *Steel Compos. Struct., Int. J.*, **24**(5), 549-559.

Moon, J., Yi, J., Choi, B.H. and Lee, H.-E. (2009), "Shear strength and design of trapezoidally corrugated steel webs" *J. Constr. Steel Res.*, **65**(5), 1198-1205.

Niea, J.-G., Zhu, L., Tao, M.-X. and Tang, L. (2013), "Shear strength of trapezoidal corrugated steel webs", *J. Constr. Steel Res.*, **85**(1), 105-115.

Pasternak, H. and Kubieniec, G. (2010), "Plate girders with corrugated webs", *J. Civil Eng. Manag.*, **16**(2), 166-171.

Sause, R. and Braxtan, T.N. (2011), "Shear strength of trapezoidal corrugated steel webs", *J. Constr. Steel Res.*, **67**(2), 223-236.

Shiratani, H., Ikeda, H., IMAI, Y. and Kano, K. (2003), "Flexural shear behavior of composite bridge girder with corrugated steel webs around middle support", *JSCE J.*, **724**(I-62), 49-67.

Timoshenko, S.P. and Gere, J.M. (1961), *Theory of Elastic Stability*, McGraw-Hil, New York, NY, USA.

Yi, J., Gil, H., Youm, K. and Lee, H. (2008), "Interactive shear buckling behavior of trapezoidally corrugated steel webs", *Eng. Struct.*, **30**(6), 1659-1666.

DL